




Evaluation of the Dielectric Properties of $\text{CaMoO}_4\text{--TiO}_2$ Composites for Microwave Applications Under Temperature Variation

Francisco Enilton Alves Nogueira^{1,6} · Tallison Oliveira Abreu^{2,6} · Vitor Carvalho Martins^{2,6} · Roterdan Fernandes Abreu^{1,6} · Felipe Felix do Carmo^{2,6} · João Paulo Costa do Nascimento^{3,6}  · Anupama Ghosh⁴ · Antonio Jefferson Manguiera Sales⁶ · Marcelo Antonio Santos da Silva⁶ · Ronaldo Santos da Silva⁵ · Antonio Sérgio Bezerra Sombra⁶

Received: 12 August 2022 / Accepted: 13 January 2023 / Published online: 8 February 2023
© The Minerals, Metals & Materials Society 2023

Abstract

This work presents experimental and numerical investigations of the microwave dielectric properties of the ceramic matrix CaMoO_4 (CMO) with the addition of 8, 12, and 20 wt% TiO_2 , obtained through the solid-state reaction method. X-ray diffraction and Rietveld's refinement revealed no evidence of secondary phases, indicating no reaction between the CMO and TiO_2 phases. The dielectric properties presented an improvement with the addition of TiO_2 , with the CMO8 sample presenting $\epsilon'_r = 12.8$, $\tan \delta = 7.8 \times 10^{-4}$, and $\tau_f = -6 \text{ ppm}^\circ\text{C}^{-1}$, demonstrating that this material has thermal stability ($\tau_f < 0$). The ceramic was tested as a dielectric resonator antenna (DRA) and numerical simulation results showed that the materials have a realized gain of 4.40–4.92 dBi, a bandwidth of 741–1079 MHz, and a radiation efficiency above 86%. The results indicate that CMO--TiO_2 systems could be employed in devices operating in the S-band.

Keywords Dielectric resonator antenna (DRA) · CMO · TiO_2 · dielectric properties · microwave

Introduction

Mobile communications, satellite communications, the global positioning system, and other communication technologies have made great advances in the field of telecommunications, and microwave dielectric materials have been widely used in microwave components such as substrates, resonators, and filters.^{1–5} Ceramic materials tend to be widely used in electronic devices due to their ability to modify their structure and adjust their dielectric properties. In general, there is a high demand for microwave dielectric ceramics with appropriate permittivity (ϵ_r), temperature coefficients of resonant frequency close to zero (τ_f), and high-quality factors ($Q \times f$) or low dielectric loss ($\tan \delta$).^{6–9}

The ceramic matrix CaMoO_4 (CMO) is a molybdate with a scheelite-type structure with space group $I41/a$.^{10,11} In CMO, molybdenum forms a tetrahedron, and calcium is coordinated by eight oxygen atoms.¹² This structure gives the CMO excellent dielectric and luminescent properties, having great potential in applications such as solid-state lasers, white-light emitting diodes, optical fibers, and humidity and microwave sensors.^{13–16}

✉ João Paulo Costa do Nascimento
jpquimico3@gmail.com

Francisco Enilton Alves Nogueira
fenilton@gmail.com
http://www.locem.ufc.br

- ¹ Telecommunication Engineering Department, Federal University of Ceará (UFC), P.O. Box 6007, Fortaleza, CE 60755-640, Brazil
- ² Department of Organic and Inorganic Chemistry, Federal University of Ceará (UFC), Fortaleza, CE, Brazil
- ³ Federal Institute of Education, Science and Technology of Ceará, PPGET, Fortaleza, CE, Brazil
- ⁴ LaMFA - Advanced Functional Materials Laboratory, Central Analítica, Physics Department, Federal University of Ceará - UFC, Fortaleza, CE 60440-554, Brazil
- ⁵ Group Functional Nanomaterials, Physics Department, Federal University of Sergipe, Sao Cristóvão, SE 49100-000, Brazil
- ⁶ Telecommunication and Materials Science and Engineering of Laboratory (LOCEM), Physics Department, Federal University of Ceará (UFC), Campus PICI, P.O. Box 6030, Fortaleza, CE, Brazil

Titanium dioxide (TiO_2) is widely used in materials science because it has good characteristics such as low dielectric loss and high dielectric permittivity.¹⁷ This oxide presents an extremely high positive temperature coefficient of resonant frequency ($\tau_f = +450 \text{ ppm}^\circ\text{C}^{-1}$), so the addition of this material in matrix ceramics with a negative τ_f could result in composites that are thermally stable ($\tau_f \geq \pm 10 \text{ ppm}^\circ\text{C}^{-1}$).^{18–20}

In this work, the effect of TiO_2 addition on the structure of CMO was analyzed by means of x-ray diffraction (XRD). Furthermore, the dielectric properties of the composites in the microwave region were analyzed, as well as the behavior of these materials acting as dielectric resonator antennae (DRA).

Experimental

Calcium molybdate (CaMoO_4) was synthesized by the solid-state reaction method through the stoichiometric mixture of calcium carbonate (CaCO_3 ; Vetec 99%) and molybdenum oxide (MoO_3 ; Sigma 99.5%). The precursor reagents were milled for 4 h at 360 rpm in a planetary mill (Fritsch Pulverisette 5) and the resulting powder was calcined in a resistive oven at 900°C for 4 h. The chemical reaction that describes the formation of CaMoO_4 is given by:



The powder was then mixed with commercial titanium oxide (TiO_2 ; Dynamica 99%) to obtain $\text{CaMoO}_{4(1-x)}\text{-TiO}_{2(x)}$ composites. The mixture was prepared in compositions of 0%, 8%, 12%, and 20% by mass of TiO_2 , and were called CMO, CMO8, CMO12, and CMO20, respectively. Then, the composites were molded in cylindrical ceramic cylinders with a uniaxial pressure of 98 MPa. Next, the green bodies were sintered in a resistive furnace at 1200°C for 4 h.

The crystalline structure analysis of the materials was performed by XRD measurements employing a diffractometer model (Rigaku D/max-B). The diffraction patterns were obtained in a range of 20° – 80° with an incident wavelength ($\text{Cu-K}\alpha 1$) of 1.5443 \AA , working at 40 kV and 40 mA, with a scan step of 0.013° . The surface morphology of the samples was investigated employing scanning electron microscopy (SEM) in a Quanta 450 FEG instrument.

The Hakki–Coleman technique was employed in the measurements of the dielectric properties of the CMO– TiO_2 composites in the microwave range, where the ceramic cylinders were manufactured following the diameter and height ratio of 2:1, which is a requirement for the Hakki–Coleman methodology.

The evaluation of the thermal stability was carried out through the method described by

Silva–Fernandes–Sombra,⁴ using an Agilent N5230A network analyzer. The temperature coefficients of the resonant frequency (τ_f) were calculated by shifting the resonant frequency with increasing temperature according to:

$$\tau_f = \frac{1}{f_0} \frac{\Delta f}{\Delta T} * 10^6 (\text{ppm}^\circ\text{C}^{-1}) \quad (2)$$

where f_0 is the resonant frequency of the $\text{HE}_{011\delta}$ mode measured at 30°C , and Δf and ΔT are the variations in resonant frequency and temperature (30 – 80°C), respectively.

Numerical simulations were performed using Ansoft HFSS[®] software to obtain the far-field parameters for all the samples. Figure 1 shows the experimental configuration used in the tests, where a ceramic cylinder is fed laterally by the coaxial cable. In this configuration, it is possible to visualize the $\text{HE}_{11\delta}$ mode whose resonant frequency equation is:

$$f_{\text{HE}_{11\delta}} = \frac{6.324c}{2\pi a \sqrt{\epsilon}} \left[0.27 + 0.36 \left(\frac{a}{2h} \right) \right] + 0.02 \left(\frac{a}{2h} \right)^2 \quad (3)$$

where a is the radius and h is the height of the cylinder ceramic, c refers to the speed of light in a vacuum and ϵ refers to the dielectric permittivity of the cylinder ceramic. From this configuration, it is possible to find a better impedance matching to obtain the far-field parameters, such as gain, efficiency, the radiation diagram, and the radiation coefficient of the DRA. In addition, the configuration in Fig. 1 shows the air gaps between the DRA and the probe and between the DRA and the ground plane, where these air gaps are inserted in the simulation to adjust and improve the impedance matching in the theoretical model in order to approximate the simulated results with those obtained experimentally.

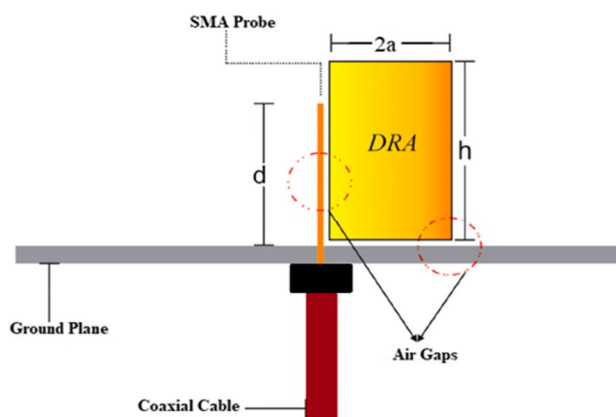


Fig. 1 Setup employed in the measurements of CMO and composites as DRA.

Results and Discussion

The comparative diffraction patterns of the CMO sample synthesized with ICSD No. 060552 (space group I 41/a) and with Rietveld refinement are presented in Fig. 2a, b. It can be observed that all the peaks of the CMO sample coincide well with the ICSD standard, whereas no additional peaks from other crystalline phases are observed. In addition, low residual values between the observed and the calculated diffraction patterns were obtained, confirming the formation of the single-phase CMO. The statistical parameters obtained by Rietveld refinement are $\chi^2 = 2.23$, R_B (%) = 6.45, and R_{wp} (%) = 4.81. These values are acceptable and indicate that the realized refinement is reliable.

Rietveld refinement was used to determine the percentage of phases present in the CMO_(1-x)-(TiO₂)_x composites, and the refined diffractograms are shown in Fig. 3. Through the analysis of the refined diffractograms, we can confirm the presence of CaMoO₄ (ICSD No. 060552) and TiO₂ (ICSD No. 024277—space group P 42/m n m) phases in all the composites, demonstrating that there was no chemical reaction between these phases. Statistical parameters from the Rietveld refinement and the mass fraction values of the composites are shown in Table I.

For all the samples, the experimental density was obtained through pycnometry, and the theoretical densities of the CMO and TiO₂ were obtained through Rietveld refinement, where CMO presents $\rho = 4.254 \text{ g cm}^{-3}$ and TiO₂

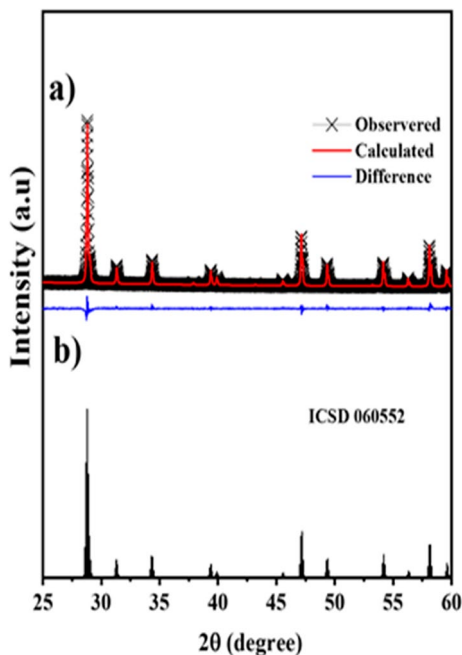


Fig. 2 (a) Rietveld refinement of CMO sample, (b) XRD comparative between CMO and ICSD pattern.

has $\rho = 4.252 \text{ g cm}^{-3}$. The results of absolute density (σ) and relative density (σ_r) can be seen in Table II and Fig. 4, where the relative density is obtained by the ratio between the experimental and theoretical densities.

It can be seen that the addition of TiO₂ provided an improvement in the relative density of the composites, reaching 91% for the CMO20. It is known from the literature that the oxide TiO₂ is employed as a sintering aid, being able to improve the relative density of ceramic materials.^{21,22}

Figure 5a–d shows SEM micrographs of the surface microstructures of the CMO–TiO₂ composites with a magnification of $\times 1000$. The morphology of the CMO presents a microstructure with grains of various shapes and sizes with well-defined boundaries, demonstrating the polycrystalline nature of this material. The increase of the TiO₂ addition resulted in a more irregular morphology of the composites, where an increase in the number of rod-like grains can be observed. In addition, no significant variation in the porosity of the materials after TiO₂ addition can be seen, which is in agreement with the densification results presented in Table II.

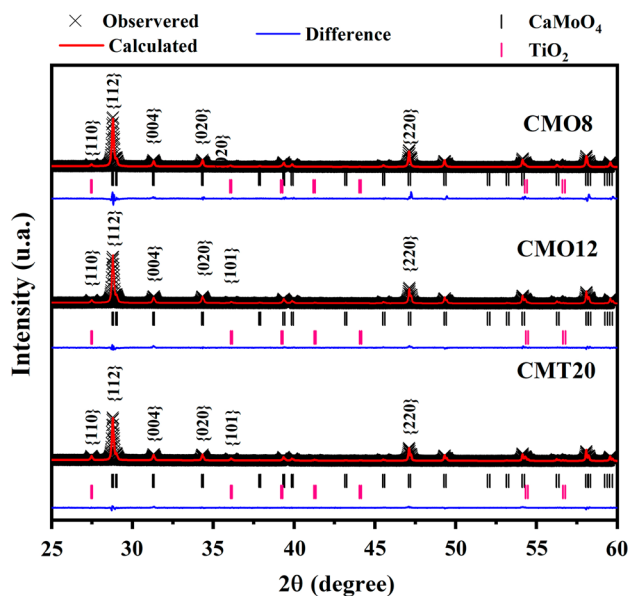


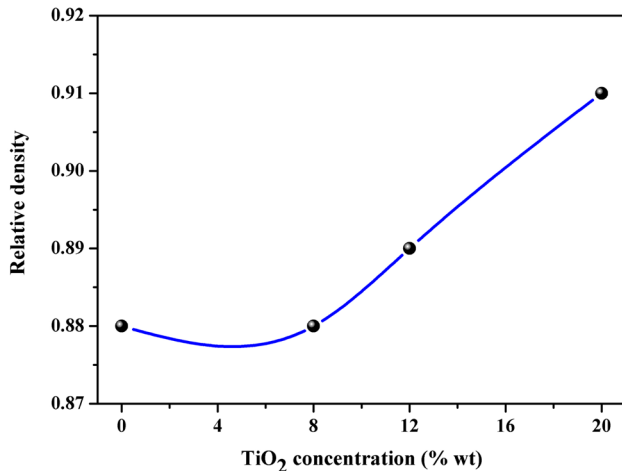
Fig. 3 Rietveld refinement of the CMO–TiO₂ composites.

Table I Parameters from Rietveld refinement and densification for all samples

Samples	Parameters			Mass fraction (%)		σ_r^a
	χ^2	R_{WP} (%)	R_B	CMO	TiO ₂	
CMO	2.23	6.45	4.81	100	0	0.88
CMO8	1.458	10.18	9.18	94.23	5.77	0.88
CMO12	1.807	5.55	8.12	89.65	10.35	0.89
CMO20	1.597	5.63	9.23	83.14	16.85	0.91

Table II Dielectric properties of CMO–TiO₂ composites

DRA	Radio (a) (mm)	Height (h) (mm)	Ratio (a/h)	ϵ'_r	$\tan\delta$	$Q \times f$	τ_f (ppm°C ⁻¹)
CMO	6.11	5.92	1.03	9.3	5.2×10^{-4}	21,604.60	- 30
CMO8	6.03	6.08	0.99	12.8	7.8×10^{-4}	12,484.03	- 6
CMO12	6.00	5.96	1.00	13.4	6.9×10^{-4}	13,510.91	+ 27
CMO20	5.98	6.00	0.99	19.0	7.3×10^{-4}	11,003.83	+ 166

**Fig. 4** Relative density variation as a function of TiO₂ addition in all the samples.

The dielectric properties in the microwave range of the CMO–TiO₂ systems were analyzed using the Hakki–Coleman technique. As observed in Fig. 6, the composites demonstrate an increase in the dielectric permittivity with the TiO₂ concentration, reaching a value of $\epsilon'_r = 19.0$ for the CMO20 composite. This can be explained by the fact that TiO₂ presents a high dielectric permittivity ($\epsilon'_r = 100$)² compared to the CMO phase ($\epsilon'_r = 9.3$). Regarding the dielectric losses ($\tan \delta$), no significant variation was observed, with all the materials showing $\tan \delta$ values in the order of 10^{-4} , since the CMO and TiO₂ phases have similar loss tangent values ($\tan \delta_{TiO_2} = 1.8 \cdot 10^{-4}$).²¹

The measurement of the resonance frequency temperature coefficient (τ_f) was performed to verify the thermal stability of the materials in the microwave region. It was observed that the CMO ceramic matrix has $\tau_f = -30$ ppm°C⁻¹, proving to be a thermally unstable material, as it is outside the acceptable range of τ_f (-10 ppm°C⁻¹ to $+10$ ppm°C⁻¹). With the addition of TiO₂, which has positive τ_f ($+450$ ppm°C⁻¹),²³ to the CMO ceramic matrix, it was possible to reach a thermal stability with a value of $\tau_f = -6$ ppm°C⁻¹ for the CMO8 sample. Figure 7 shows the variation of τ_f with the addition of TiO₂ in the composites investigated.

The manufactured ceramic cylinder was tested as a DRA, while numerical simulations were performed to obtain the far-field parameters of the CMO–TiO₂ composites.

The experimental and theoretical return loss (S_{11}) are shown in Fig. 8, where it can be seen that the samples have a reflection coefficient below -10 dB, demonstrating that they could operate as DRA.^{24,25} It is noted that the frequency of operation of the DRAs decreases with the increase of the percentage of TiO₂. This can be explained by the fact of the high permittivity of TiO₂ causing an increase of ϵ'_r of the DRAs (as observed in Table II), consequently resulting in the decrease of the frequency of the materials investigated. The bandwidth calculated for the CMO at -10 dB was equal to 1079 MHz, while, for the composites studied, the bandwidth value decreased, with a lower value being observed of 741 MHz for the CMO20 system.

Figure 9 shows the components of the real and imaginary impedances, where it can be seen that the differences between the experimental and simulated curves are small, indicating an excellent fit. In addition, a small shift in the peak resonance frequency between the composites is observed for the DRAs.

Table III shows the characteristics of the transmission lines and the impedance lines obtained by the relationship $Z = R + jX$. The results show that the impedance values are close to the characteristic impedance value of 50Ω ; that is, it can be considered that, at the respective resonance frequencies, all the antennae can achieve maximum power transfer.²⁶ The reflection coefficient (Γ) and the voltage standing wave ratio (VSWR) locate the impedance for CMO at the resonant frequency of 6.05 GHz, with $Z (\Omega) = 50.5 - j0.37$. The CMO matrix has a low reflection coefficient of $\Gamma = 0.003$. The angle was -0.42° , indicating that the wave travels from the source to the load, the calculated radiation efficiency was 99%, and the VSWR was 1.05, indicating that the power transmitted by the antenna was satisfactory with little reflection. These results are important specifications for microwave components.⁷

The CMO8 and CMO12 composites presented excellent radiation efficiency results, both with 99% and with VSWM = 1.02 and 1.01, respectively. Moreover, the CMO, CMO8, and CMO12 presented negative $X(\Omega)$ values, which implies that the materials have a capacitive reactance, and with negative angles, indicating that the wave travels from the source to the load. The CMO12

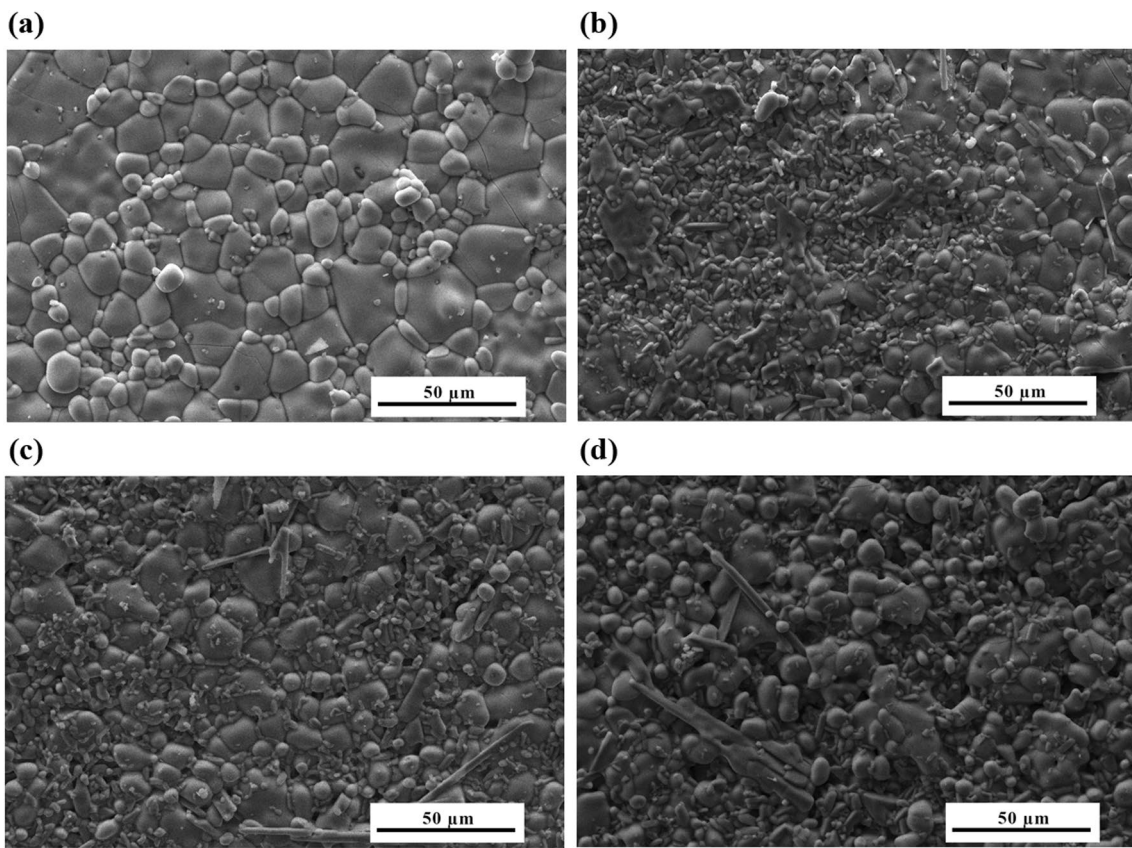


Fig. 5 SEM micrographs at room temperature with a magnification factor of ×1000 for: (a) CMO, (b) CMO8, (c) CMO12, and (d) CMO20.

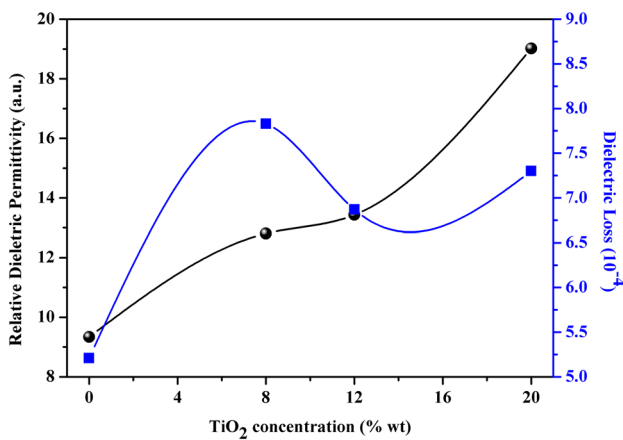


Fig. 6 Permittivity (ϵ_r) and dielectric loss ($\tan \delta$) values obtained for CMO-TiO₂ system in the microwave range.

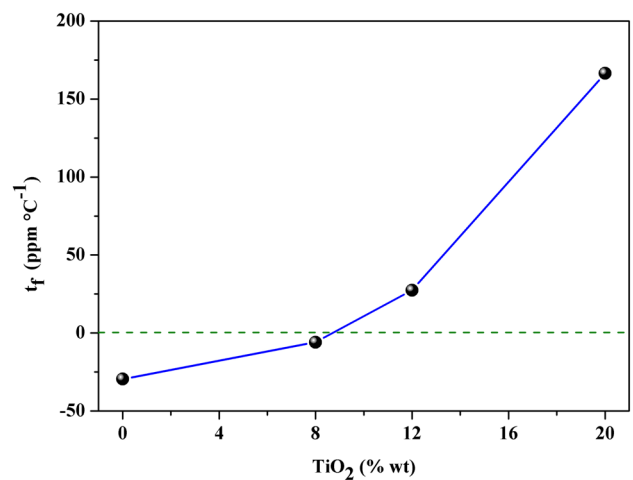


Fig. 7 Temperature coefficient of resonant frequency of CMO-TiO₂ composites.

composite has a $Z(\Omega) = 49.3 + j0.1$, presenting an inductive reactance, and with an angle of $+0.22^\circ$, indicating that the wave is in the direction of the load. The calculated

radiation efficiency was 99% with a $\Gamma = 0.007$. Through the results obtained and presented in Table III, it was observed that the influence of TiO₂ in the CMO matrix

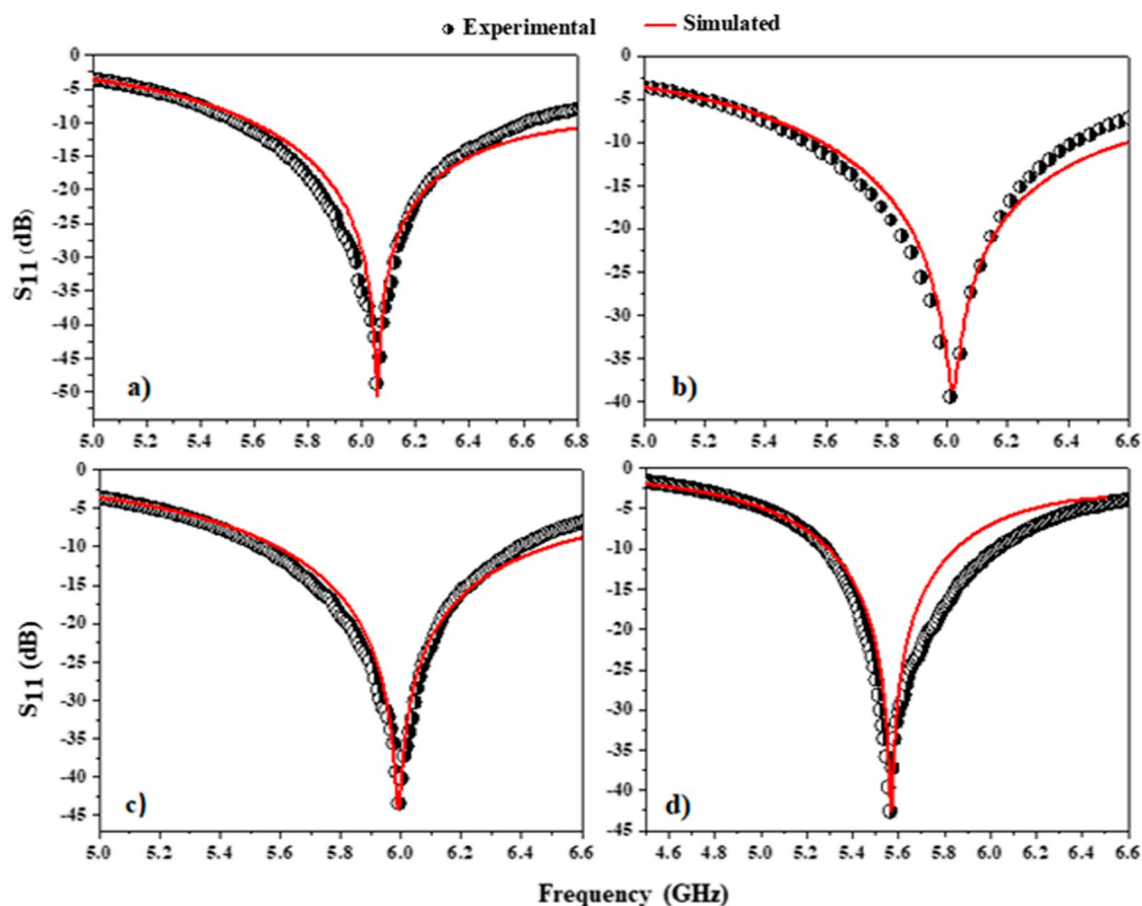


Fig. 8 Experimental and theoretical return loss (S_{11}) for all samples: (a) CMO, (b) CMO8, (c) CMO12, and (d) CMO20.

makes the composites leave a capacitive reactance and go to inductive reactance.

With the good fit between the experimental and simulated data shown in Figs. 8 and 9, the values of the far-field parameters were obtained and the results are shown in Table IV. Addition of TiO_2 to the CMO ceramic matrix provided improvements in the antenna parameters of the realized gain and radiation efficiency, where the CMO20 presented the best results compared with the other materials, presenting a gain of 3.11 dB and radiation efficiency of 99.7%.

Table V presents far-field parameters of other thermally stable systems used for the manufacture of DRAs, where it is possible to observe that CMO20 has values near to or greater than those presented by many materials reported in the literature. These results demonstrate that CMO– TiO_2 composites have potential application as DRAs and/or other devices that operate in the S-band, such as communication satellites, Wi-Fi devices, and weather radar.^{25,27}

Conclusions

The dielectric properties of the CMO (CaMoO_4) ceramic matrix with the addition of TiO_2 have been analyzed. X-ray diffraction and Rietveld's refinement demonstrated the presence of the CMO and TiO_2 phases in the system, demonstrating that there was no formation of secondary phases.

It was observed that, with the addition of TiO_2 , the permittivity increased, while the tangent of loss hardly changed. The increase of permittivity resulted in the decrease of the operating frequency of DRAs from 6.05 GHz to 5.56 GHz. In addition, the addition caused an increase in the τ_f values of the samples, with CMO8 demonstrating the value closest to zero ($\tau_f = -6 \text{ ppm}^\circ\text{C}^{-1}$).

Numerical simulation was employed to obtain the far-field parameters of the CMO– TiO_2 composites, where

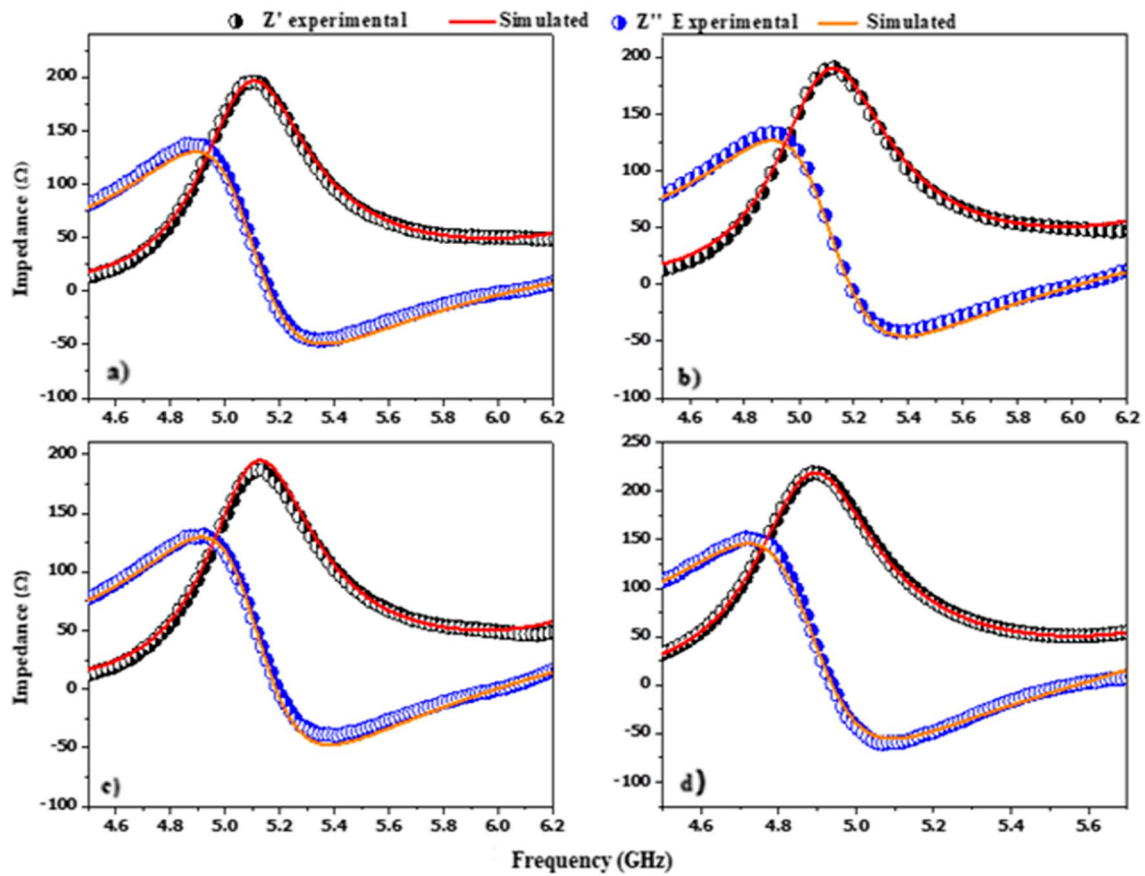


Fig. 9 Real and imaginary impedances experimental and simulated for: (a) CMO, (b) CMO8, (c) CMO12, and (d) CMO20.

Table III Far-field parameters obtained for all the samples

DRA	CMO	CMO8	CMO12	CMO20
Frequency (GHz)	6.05	6.00	5.99	5.56
Realized gain (dBi)	4.40	4.77	4.82	4.92
Radiation efficiency (%)	86.1	99.5	99.5	99.7
Bandwidth (MHz)	1079	891	860	741
Bandwidth (%)	17.83	14.85	14.36	13.33

Table IV Parameters obtained by the experimental impedance of the samples

DRA	R (Ω)	X (Ω)	VSWR	Γ	T (%)	Angle (°)	Γ _{pwr} (%)
CMO	50.5	-0.37	1.00	0.003	0.99	-0.42	0.001
CMO8	49	-0.22	1.02	0.010	0.99	-0.26	0.010
CMO12	49.4	-0.31	1.01	0.006	0.99	-0.36	0.004
CMO20	49.3	0.19	1.01	0.007	0.99	0.22	0.005

Table V Values of far-field parameters values of different ceramics composites

Material	Reference	Gain (dBi)	Efficiency (%)	BW (MHz)
Ba(Zn _{1/3} Ta _{2/3})O ₃ – Cr ₂ O ₃ (BZTCR1)	25	6.40	80.00	290
YNbO ₄ – CaYTiNbO ₇ (YCT15%)	27	5.10	95.88	129
Y ₃ Fe ₅ O ₁₂ – CaTiO ₃ (YIG _{0.25} CTO _{0.75})	28	3.91	96.24	103
BiVO ₄ – CaTiO ₃ (BV16)	29	5.93	91.44	130
LTCN _{0.2} + 3 wt% H ₃ BO ₃	30	4.03	93.00	600
CaMoO ₄ – TiO ₂ (CMO20)	Present work	4.92	99.7	741

it was observed that the samples demonstrated a realized gain above 2.70 dBi, a bandwidth between 741 and 1079 MHz, and a radiation efficiency ranging between 86.1 and 99.7%. The values presented here demonstrate that the ceramic materials investigated could be employed in devices operating in the S-band, such as in telecommunications and in surface ship and weather radars.

Funding This work was partly sponsored by the Brazilian Research Agencies CNPq-Conselho Nacional de Desenvolvimento Científico e Tecnológico (Grant INCT NANO(BIO)SIMES), CAPES—Coordenação de Aperfeiçoamento de Pessoal de Ensino Superior (Grant Project PNPD), FINEP-Financiadora de Estudos e Projetos (Grant INFRAPESQ-11 and INFRAPESQ-12), and the U.S. Air Force Office of Scientific Research (AFOSR) (FA9550-16-1-0127).

Availability of Data and Materials Not applicable.

Code Availability Not applicable.

Conflict of Interest The authors declare that they have no conflict of interest.

References

1. S. Parida, S.K. Rout, V. Subramanian, P.K. Barhai, N. Gupta, and V.R. Gupta, *J. Alloys Compd.* 528, 126 (2012).
2. M.T. Sebastian, *Dielectric Materials for Wireless Communication*, 1st ed., (Oxford: Elsevier, 2008).
3. S. George and M.T. Sebastian, *J. Am. Ceram. Soc.* 93, 2164 (2010).
4. M.A.S. Silva, T.S.M. Fernandes, and A.S.B. Sombra, *J. Appl. Phys.* 112, 074106 (2012).
5. G. Kaur, K. Pubby, S. Bahel, and S.B. Narang, *Ceram. Int.* 44, 20484 (2018).
6. W. Liu and R. Zuo, *J. Eur. Ceram. Soc.* 38, 119 (2018).
7. T.O. Abreu, R.F. Abreu, F.F. do Carmo, W.V. de Sousa, H.O. de Barros, J.E.V. de Morais, J.P.C. do Nascimento, M.A.S. da Silva, S. Trukhanov, A. Trukhanov, L. Panina, C. Singh, and A.S.B. Sombra, *Ceram. Int.* 47, 15424 (2021).
8. V.C. Martins, R.G.M. Oliveira, F.F. Carmo, M.A.S. Silva, S.A. Pereira, J.C. Goes, M.M. Costa, D.X. Gouveia, and A.S.B. Sombra, *J. Phys. Chem. Solids* 125, 51 (2019).
9. X. Hu, J. Jiang, J. Wang, L. Gan, and T. Zhang, *J. Mater. Sci. Mater. Electron.* 31, 2544 (2020).
10. E. Sinha and P. Yadav, *Ferroelectrics* 517, 1 (2017).
11. E.C. Xiao, Q. Ren, Z. Cao, G. Dou, Z.M. Qi, and F. Shi, *J. Mater. Sci. Mater. Electron.* 31, 5686 (2020).
12. T. Qin, Q. Wang, D. Yue, W. Shen, Y. Yan, Y. Han, Y. Ma, and C. Gao, *J. Alloys Compd.* 730, 1 (2018).
13. C. Bouzidi, K. Horchani-Naifer, Z. Khadraoui, H. Elhouichet, and M. Ferid, *Phys. B Condens. Matter* 497, 34 (2016).
14. F. Huang, Y. Gao, J. Zhou, J. Xu, and Y. Wang, *J. Alloys Compd.* 639, 325 (2015).
15. P. Dixit, V. Chauhan, S.B. Rai, and P.C. Pandey, *J. Alloys Compd.* 897, 162820 (2022).
16. A.A.G. Santiago, E.M. Macedo, F.K.F. Oliveira, R.L. Tranquilin, M.D. Teodoro, E. Longo, F.V. Motta, and M.R.D. Bomio, *Mater. Res. Bull.* 146, 111621 (2022).
17. E.A. Moore and L.E. Smart, *Solid State Chemistry: An Introduction*, 4th ed., (Boca Raton: CRC Press, 2012).
18. K. Shigeno, M. Li, and H. Fujimori, *J. Eur. Ceram. Soc.* 41, 376 (2021).
19. Z. Wang, L. Liu, Q. Du, R. Tang, J. Ai, and Y. Chen, *Ceram. Int.* 48, 14378 (2022).
20. Z. Weng, C. Song, Z. Xiong, H. Xue, W. Sun, Y. Zhang, B. Yang, M.J. Reece, and H. Yan, *Ceram. Int.* 45, 13251 (2019).
21. M.A.S. Silva, R.G.M. Oliveira, and A.S.B. Sombra, *Ceram. Int.* 45, 20446 (2019).
22. Y. Yang, Q. Chang, Z. Hu, and X. Zhang, *Membranes* 8, 49 (2018).
23. J.E.V. de Morais, R.G.M. de Oliveira, A.J.N. de Castro, J.C. Sales, M.A.S. Silva, J.C. Goes, M.M. Costa, and A.S.B. Sombra, *J. Electron. Mater.* 46, 5193 (2017).
24. D.V.M. Paiva, M.A.S. Silva, A.S.B. Sombra, and P.B.A. Fechine, *J. Alloys Compd.* 748, 766 (2018).
25. M. Haydoura, R. Benzerga, C. Le Paven, L. Le Gendre, V. Laur, A. Chevalier, A. Sharaiha, F. Tessier, and F. Cheviré, *J. Alloys Compd.* 872, 159728 (2021).
26. R.G.M. Oliveira, J.E.V. de Morais, D.C. Souza, M.A.S. Silva, D.X. Gouveia, S. Trukhanov, A. Trukhanov, L. Panina, C. Singh, D. Zhou, and A.S.B. Sombra, *J. Aust. Ceram. Soc.* 57, 369 (2021).
27. F.F. do Carmo, J.P.C. do Nascimento, J.E.V. de Morais, V.C. Martins, J.C. Sales, M.A.S. Silva, R.S. Silva, and A.S.B. Sombra, *Mater. Chem. Phys.* 271, 124956 (2021).
28. D.V.M. Paiva, M.A.S. Silva, R.G.M. de Oliveira, A.R. Rodrigues, L.M.U.D. Fechine, A.S.B. Sombra, and P.B.A. Fechine, *J. Alloys Compd.* 783, 652 (2019).
29. R.G.M. Oliveira, R.A. Silva, J.E.V. de Morais, G.S. Batista, M.A.S. Silva, J.C. Goes, H.D. de Andrade, I.S. Queiroz Júnior, C. Singh, and A.S.B. Sombra, *Compos. Part B Eng.* 175, 107122 (2019).
30. H.-H. Guo, M.-S. Fu, D. Zhou, C. Du, P.-J. Wang, L.-X. Pang, W.-F. Liu, A.S.B. Sombra, and J.-Z. Su, *ACS Appl. Mater. Interfaces* 13, 912 (2021).

Publisher's Note Springer Nature remains neutral with regard to jurisdictional claims in published maps and institutional affiliations.

Springer Nature or its licensor (e.g. a society or other partner) holds exclusive rights to this article under a publishing agreement with the

author(s) or other rightsholder(s); author self-archiving of the accepted manuscript version of this article is solely governed by the terms of such publishing agreement and applicable law.